BECKER, P. & COPPENS, P. (1974). *Acta Cryst.* A**30**, 129–147; 148–153.
BECKER, P. & COPPENS, P. (1975). *Acta Cryst.* A**31**, 417–425.
BOND, W. L. (1960). *Acta Cryst.* **13**, 814–818.
BUCKINGHAM, A. D. (1959). *Q. Rev.* **13**, 183–214.
CHELIKOWSKY, J. R. (1977). *Solid State Commun.* **22**, 351–354.
COMMISSION ON NEUTRON DIFFRACTION (1982). December Newsletter.
CRAVEN, B. M. & WEBER, H. P. (1987). Private communication.
DESLATTES, R. D. & HENINS, A. (1973). *Phys. Rev. Lett.* **31**, 972–975.
DONNAY, G. (1985). *Can. Mineral.* **23**, 655–658.
GROUT, P. J., MARCH, N. H. & LEWIS, J. W. E. (1981). *Ferroelectrics*, **33**, 167–172.
HAMILTON, W. C. (1965). *Acta Cryst.* **18**, 502–510.
HEILAND, G. & IBACH, H. (1966). *Solid State Commun.* **4**, 353–356.
KARPPINEN, M., LIMINGA, R., KVICK, Å & ABRAHAMS, S. C. (1988). *J. Chem. Phys.* **88**, 351–355.
KIHARA, K. & DONNAY, G. (1985). *Can. Mineral.* **23**, 647–654.
LAUDISE, R. A., KOLB, E. D. & CAPORASO, A. J. (1964). *J. Am. Ceram. Soc.* **47**, 9–12.
LIMINGA, R., ABRAHAMS, S. C., GLASS, A. M. & KVICK, Å. (1982). *Phys. Rev. B*, **26**, 6896–6900.
LUNDGREN, J.-O. (1982). Report UUIC-B13-4-05. Institute of Chemistry, Univ. of Uppsala, Sweden.
NYE, J. F. (1957). *Physical Properties of Crystals*. Oxford Univ. Press.
O'BRYAN, H. M., VAN UITERT, L. G., KOLB, E. D. & ZYDIK, G. (1978). *J. Am. Ceram. Soc.* **61**, 269.
PHILLIPS, J. C. (1973). *Bonds and Bands in Semiconductors*. New York: Academic Press.
ROBIE, R. A. & EDWARDS, J. L. (1966). *J. Appl. Phys.* **37**, 2659–2663.
STEVENS, E. D. (1974). *Acta Cryst.* A**30**, 184–189.
SVENSSON, C., ALBERTSSON, J., LIMINGA, R., KVICK, Å. & ABRAHAMS, S. C. (1983). *J. Chem. Phys.* **78**, 7343–7352.
THORNLEY, F. R. & NELMES, R. J. (1974). *Acta Cryst.* A**30**, 748–757.
TOKAREV, E. F., KARYAKINA, N. F., KOBYAKOV, I. B., KUZ'MINA, I. P. & LOBACHEV, A. N. (1973). *Izv. Akad. Nauk SSSR Ser. Fiz.* **37**, 2401–2403.
TOKAREV, E. F., KOBYAKOV, I. B., KUZ'MINA, I. P., LOBACHEV, A. N. & PADO, G. S. (1975). *Fiz. Tverd. Tela (Leningrad)*, **17**, 980–986.
TOULOUKIAN, Y. S., KIRBY, R. K., TAYLOR, R. E. & LEE, T. Y. R. (1977). *Thermophysical Properties of Matter*, Vol. 13. *Thermal Expansion*. New York: IFI/Plenum.

Acta Cryst. (1989). B**45**, 40–45

Long-Period Tetragonal Lattice Formation by Solid-State Alloying at the Interfaces of Bi–Mn Double-Layer Thin Films

BY KENTAROH YOSHIDA, TAKASHI YAMADA AND YOSHIHISA TANIGUCHI

Department of Applied Physics, Faculty of Engineering, Kobe University, Rokkodai, Nada, Kobe 657, *Japan*

(*Received* 18 *April* 1988; *accepted* 19 *September* 1988)

Abstract

Thin Bi–Mn double-layer films, consisting of a Bi layer of 300 Å in thickness and an Mn layer of 200 Å prepared by successive vacuum deposition, were heated at 538 K for 100–200 h. Transmission electron micrographs show that a long-period tetragonal lattice forms at their interfaces, whose lattice constants were $a = 17{\cdot}26$, $c = 10{\cdot}21$ Å. Near to the tetragonal lattice grains, structures preliminary to lattice formation were observed. Their electron diffraction and high-resolution micrographs show that the formation process can be divided into two stages. In the first stage, Bi and Mn atoms combine to form polyatomic clusters 16 Å in diameter, which have a twelvefold symmetry axis normal to the (001) surface of the Bi crystals. In the second stage, these polyatomic clusters arrange themselves to build up the long-range tetragonal order.

Introduction

Thin films of ferromagnetic MnBi alloy phases have been investigated because of their magneto-optic applications (Williams, Sherwood, Foster & Kelley, 1957). Unger & Stolz (1971) and Chen (1971) deposited a Bi layer onto a cleaved surface of mica and then an Mn layer onto the Bi layer. They heated this composite double-layer film at around 573 K for a few days. The present authors also prepared alloy films by the same procedure, but their samples were kept very thin (about 500 Å in total thickness) and were deposited onto very thin carbon films to allow transmission electron microscope observations. After heating of these thin composite films at 538 K for 100–200 h, the micrographs showed that the alloying process is not so simple as had been presumed. In the previous investigations of Unger & Stolz (1971), Chen (1971) and others (Iwama, Mizutani & Humphrey, 1972; Honda & Kusuda, 1974), Mn atoms were considered simply to diffuse into the underlying Bi crystals to form the MnBi crystal lattices. In the present thin specimen heated at low temperature, however, a number of long-period crystal lattices were found to appear during heating (Yoshida, Yamada & Taniguchi, 1987). Results concerning one of them, a tetragonal lattice, and its related structure are reported here.

0108-7681/89/010040-06$03.00

Experimental

The vacuum deposition chamber was evacuated by an oil diffusion pump coupled with a mechanical pump, whose ultimate pressure is about 10^{-7} Torr (1 Torr $= 1{\cdot}333 \times 10^2$ Pa). Bi and Mn were evaporated from their respective tantalum boats onto electron microscope specimen grids covered with carbon films of 100 Å in thickness. By rotating a disk shutter with a semicircular aperture cut in it, a Bi layer of about 300 Å in thickness was first deposited and an Mn layer of about 200 Å was then deposited onto the top surface of the Bi layer. Their thicknesses were measured by multiple-beam interferometry of single-metal parts of a film formed at both sides of a small screen (Yoshida, Yamada & Furukawa, 1986). The Mn deposition was performed immediately after the Bi deposition, since it was important to keep the surface of the Bi layer as clean as possible before Mn deposition. The vacuum during Bi deposition was about 10^{-6} Torr and that during Mn deposition was higher than 5×10^{-5} Torr. It should be mentioned here that the same results were obtained for a few specimens which were prepared in an ultrahigh vacuum higher than 10^{-8} Torr. The purities of the raw metals used for the depositions were 99·999% for Bi and 99·99% for Mn, respectively. After these two depositions, the specimen heater was turned on without breaking the vacuum and the composite films were heated at about 538 K, slightly below the melting point of Bi (544 K), for 100–200 h in a vacuum of 10^{-6} Torr. They were then furnace-cooled, removed from the vacuum and examined under a JEM-200CX electron microscope.

Results

When pure Bi layers without Mn deposition were heated at 538 K for 200 h, their crystal grains grew large, 0·5 μm in diameter, leaving small holes at triple, or multiple, points of their boundaries. Most of the grains were in [001] orientation when expressed in hexagonal indices, and only a few small grains were in other orientations. When the double-layer films were observed after the heat treatment, interesting features were revealed, even in the conventional bright-field micrographs. Fig. 1 shows one such micrograph for a specimen heated at 538 K for 100 h. The inset shows the back focal plane of the objective lens when Fig. 1 was taken. Several weak, but distinct, electron beams are observed to pass through the smallest objective aperture of the microscope, whose radius corresponds to 6 Å. Grain boundaries of Bi crystals are seen near both sides of Fig. 1. Parallel fringes are seen at each of the black patches, which are Mn lumps that have coagulated during heating. Most will be Moiré fringes and some of the weak beams in the inset will correspondingly have arisen from double diffraction of electrons by the overlapping lattices at their interfaces. However, there are fringes which are too straight and too well defined to be regarded as Moiré fringes. Examples can be seen in the central part of Fig. 1. A similar set of fringes at a larger magnification, photographed through the smallest objective aperture and from a specimen heated at 538 K for 200 h, is shown in Fig. 2. It is difficult to conclude that the several sets of straight and sharp parallel stripes in Fig. 2 are Moire fringes. Some long-period crystal lattices have developed at the interface during the heating: the diffracted beams from these lattices passed through the aperture and produced these images.

Single-crystalline-net electron diffraction patterns could be taken from these small black patches using a very small selected-area diffraction aperture, which had a diameter of 7 μm. Four such net patterns, taken from a specimen heated at 538 K for 168 h, are shown in

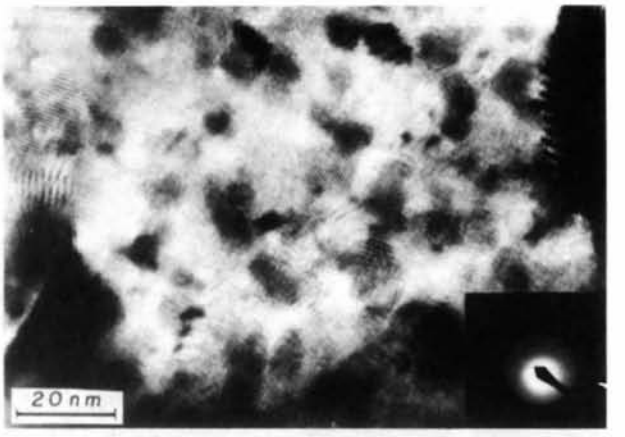

Fig. 1. Bright-field electron micrograph of a Bi–Mn double-layer film heated at 538 K for 100 h. The objective aperture shown in the inset is the smallest one ($1/6$ Å^{-1} in radius) and several beams are observed to pass through this aperture.

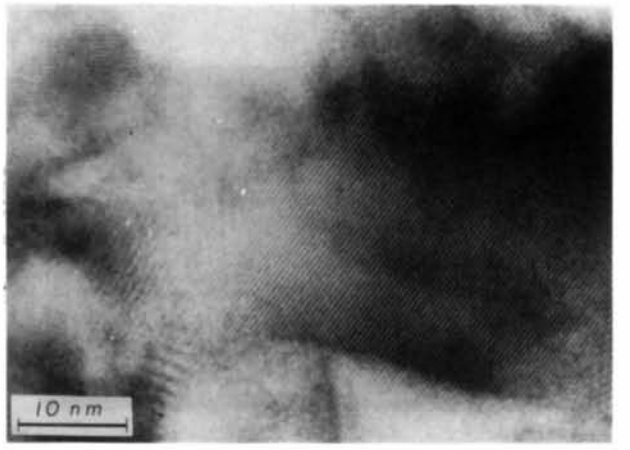

Fig. 2. Examples of parallel, sharp and straight fringes in bright-field images. The specimen was heated at 538 K for 200 h and the aperture is the same as that of Fig. 1.

Figs. 3(*a–d*). The spots are arranged in fourfold symmetry and the closest four spots to the origin have an interplanar spacing of 17·26 Å in Fig. 3(*a*). The same rows of close spots, with a spacing corresponding to 17·26 Å, are seen in the other three patterns. Figs. 3(*b–d*), in horizontal directions. It is concluded that one of them passing through the origin is the common intersection of all four patterns, Figs. 3(*a–d*), in reciprocal space. By drawing a triangle on a plane passing through the origin normal to this intersection line using the distance from the origin to a spot 030 in Fig. 3(*a*) as the base of the triangle and the two distances to a spot 051 in Fig. 3(*b*) and to a spot 021 in Fig. 3(*c*) as its remaining two sides, it was found that the top vertex of the triangle comes to a position vertically above one of the spots in Fig. 3(*a*), showing that the three-dimensional reciprocal lattice giving these patterns is tetragonal. Calculations show that its c^* axis is equal to $1/10{\cdot}21$ Å^{-1} in length and Fig. 3(*a*) constitutes its basal plane, in which the two a^* axes are taken to be from the origin to the spots, 100 and 010, respectively. Indices given in the four patterns were based on this tetragonal lattice.

Discussion

Transformation of the reciprocal lattice derived above into real space gives a tetragonal crystal lattice with unit-cell parameters,

$$a = 17{\cdot}26, \quad c = 10{\cdot}21 \text{ Å}. \qquad (1)$$

In the above construction of the reciprocal lattice, however, Fig. 3(*d*) was not used at all. This pattern, which also contains the intersection line, can be used to verify the lattice. An interplanar spacing corresponding to the measured distance to a spot, 032, in Fig. 3(*d*) is

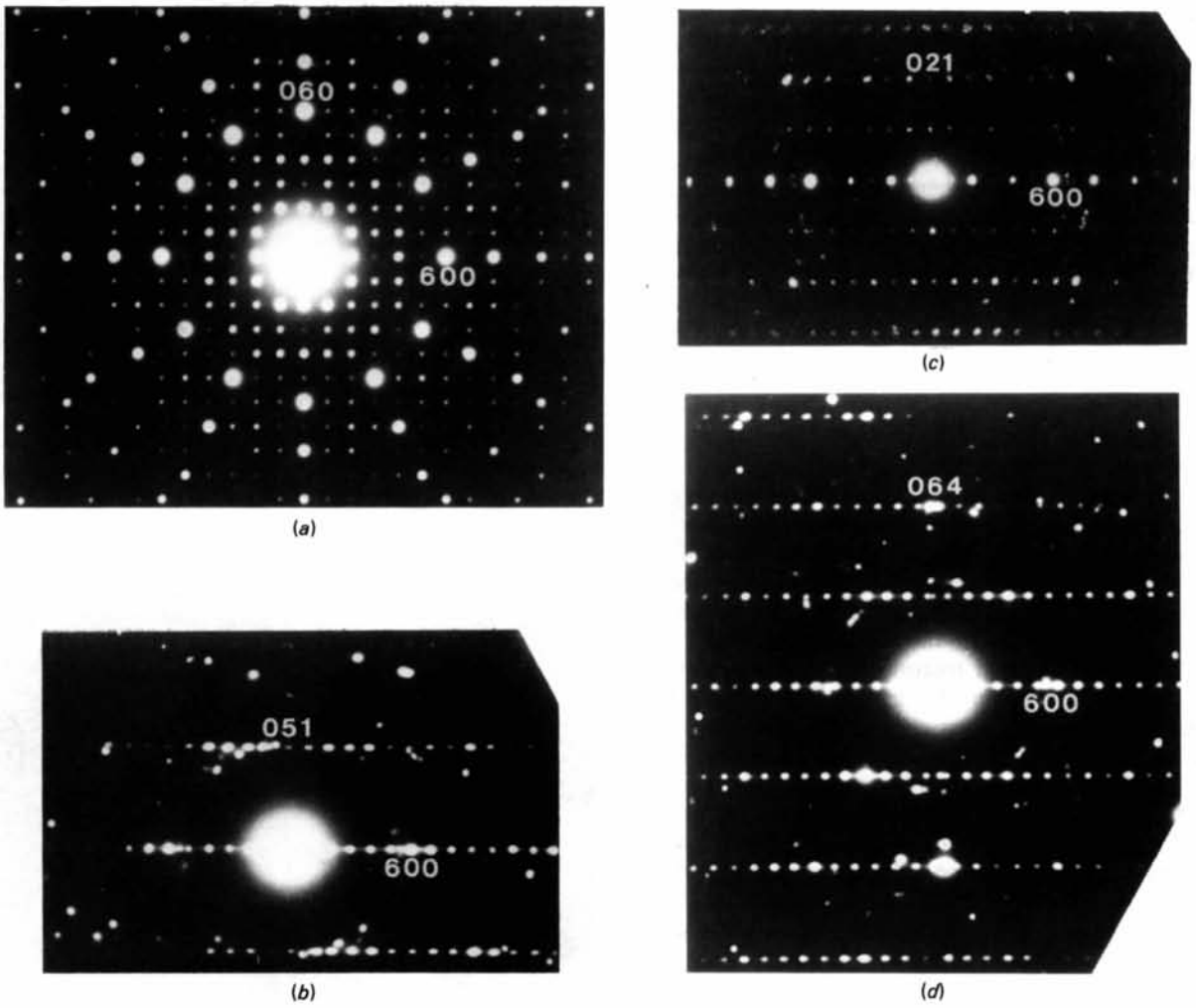

Fig. 3. (*a*)–(*d*) Single-crystalline-net electron diffraction patterns of a specimen heated at 538 K for 168 h: (*a*) constitutes the basal plane of a tetragonal reciprocal lattice and all four patterns have the same row of spots along a horizontal line passing through the origin, which is the common intersection line for all four patterns.

Table 1. *Comparison of the interrow spacings of spot rows with the tetragonal lattice,* $a = 17{\cdot}26$, $c = 10{\cdot}21$ Å

Diffraction pattern	Observed spacing (Å)	Calculated spacing (Å)	h k l
Fig. 3(*a*)	17·26	17·26	0 1 0
Fig. 3(*b*)	3·270	3·270	0 5 1
Fig. 3(*c*)	6·740	6·591	0 2 1
Fig. 3(*d*)	3·749	3·819	0 3 2
(i)	4·045	3·975	0 4 1
(ii)	1·885	1·885	0 9 1
(iii)	2·258	2·333	0 3 4

compared in Table 1 with the calculated value from the lattice (1). Agreement between both values is good. In Table 1, all other observed patterns, (i), (ii) and (iii), which also have the common intersection line, but are not shown here for economy of space, are similarly compared with the reciprocal lattice (1) and the agreements are reasonably good. Thus, a long-period tetragonal lattice (1) was found to develop in the Bi–Mn double-layer films heated at 538 K for approximately 150 h.

Fig. 4 is a high-resolution structure image of the tetragonal lattice (1) along [001]. As is seen in the inset, the objective aperture has a radius of 2·5 Å; diffracted beams with Miller indices of $d = 2{\cdot}37$ Å actually grazed the aperture and a number of beams, as many as 177 including 000, were allowed to pass through the aperture. Although somewhat faint, square unit patterns were observed to repeat in Fig. 4. Sides of these units were 16·2 and 15·9 Å, which are the mean values of the measurements at different points in Fig. 4 divided by its magnification. These sizes of the square units agree with the lattice constants (1), since the present microscope always indicates a slightly larger magnification than the one derived from diffraction patterns. The repeated square unit patterns in Fig. 4 are, therefore, a projection of the lattice (1) onto its basal plane (001).

From specimen areas near the tetragonal lattice grains, other interesting images were occasionally obtained. One of them is shown in Fig. 5, where the inset shows the beams used to produce the image. Doughnut-shaped white contrasts, 16 Å in diameter, are seen in an upper central region of Fig. 5, but they do not form any regular lattices. An optical transform from this region gives twelve spots arranged in twelvefold symmetry. The diffraction pattern from Fig. 5 for the overall region is shown in Fig. 6. Although Fig. 6 may seem, at first sight, to be similar to Fig. 3(*a*), one main difference is that the spots are arranged in twelvefold symmetry in Fig. 6, whereas they are in exact fourfold symmetry in Fig. 3(*a*). Interplanar spacings of the spots on a horizontal line through the origin in Fig. 6 are, for example, compared in Table 2

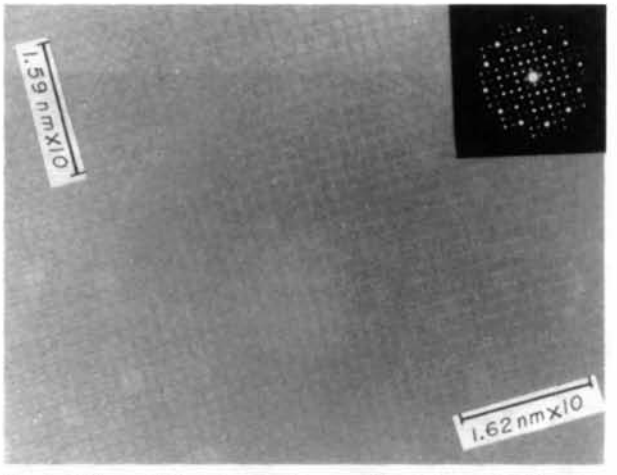

Fig. 4. High-resolution structure image of the tetragonal lattice. The specimen is the same as that in Fig. 3. The incident beam is along [001] and all beams allowed to pass through the objective aperture ($1/2{\cdot}5$ Å^{-1} in radius) are shown in the inset.

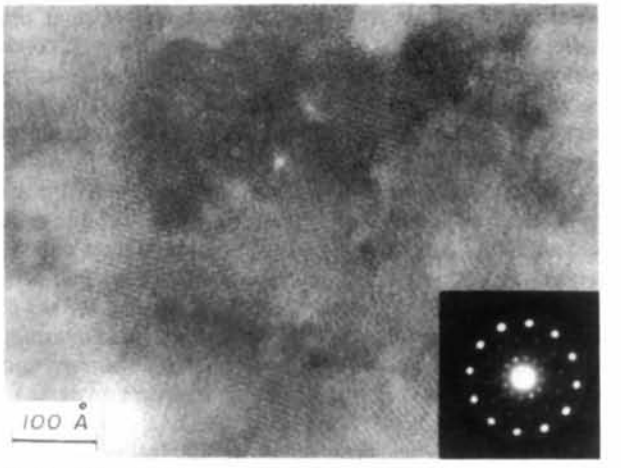

Fig. 5. High-resolution structure image of a specimen region near Fig. 4. The back focal plane of the objective lens for this image is shown in the inset.

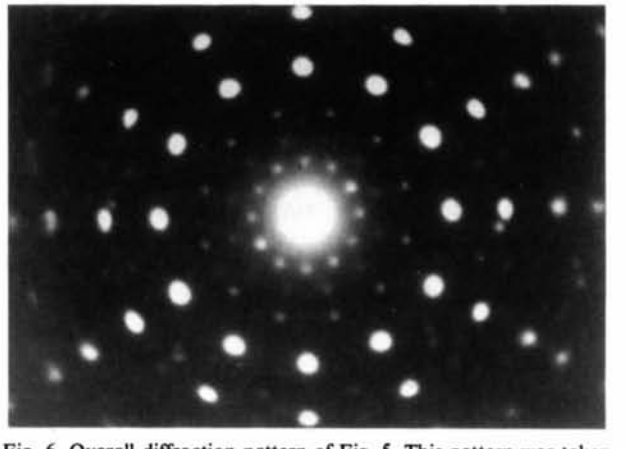

Fig. 6. Overall diffraction pattern of Fig. 5. This pattern was taken from a large area with Fig. 5 at its center.

Table 2. *Comparison of interplanar spacings* (Å) *of spots in Fig.* 6 *with those in Fig.* 3(*a*)

The interplanar spacings in Fig. 6 were measured on the horizontal line; the corresponding spots in Fig. 3(*a*) were calculated on the tetragonal lattice defined in (1).

Fig. 6	Fig. 3(*a*)
7·727 (*S*)	8·630 (200)
5·463 (*W*)	5·456 (310)
4·036 (*W*)	4·068 (330)
2·877 (*VS*)	2·877 (600)
2·331 (*W*)	
2·122 (*M*)	
2·101 (*S*)	2·158 (800)
1·603 (*S*)	1·726 (1000)
1·429 (*M*)	1·438 (1200)

with those of the spots in Fig. 3(*a*) also on the same line. The most intense spot was assigned the *hkl* indices 600 ($d = 2{\cdot}877$ Å) of the tetragonal lattice. Attempts to index other spots in Fig. 3(*a*) always led to smaller measured values than those for the tetragonal lattice. Weak and medium intensity spots which are near the horizontal line can be given the indices of the tetragonal lattice only when their interplanar spacings are compared, but their assigned indices, 310 and 330, show that they should not come very near to the horizontal line.

The structures of Figs. 5 and 6 cannot, therefore, be considered as the tetragonal lattice (1), but may be related to it. A fact that twelvefold symmetry can be expressed as $4 \times 3 = 12$ suggests this relation. This was confirmed by a specimen which was heated at 513 K for 100 h in a vacuum of 10^{-8} Torr. Its structure image is shown in Fig. 7. As will be seen, both the square unit patterns in Fig. 4 and the doughnut-shaped contrasts in Fig. 5 coexist in Fig. 7. It should also be noted that the square unit patterns form the tetragonal lattices in three different regions, *a*, *b* and *c*, which make an angle of 120° with each other. Among the diffraction patterns taken from the specimen shown in Fig. 4, a pattern showing this feature was found. This transform is shown on a larger scale in Fig. 8 to illustrate the detail of the inner spots. Each of the twelve spots nearest to the origin can clearly be recognized to consist of three spots, corresponding to the three tetragonal regions, *a*, *b* and *c*, in Fig. 7. The strongest and the largest spots in Fig. 8 can also reasonably be regarded as consisting of three spots. To test this interpretation, the regular tetragonal pattern of Fig. 3(*a*) was rotated by ±120° and the resulting three patterns were superimposed. This synthesized diffraction diagram agrees very well with Fig. 8 including its spot intensities.

Concluding remarks

The structures shown in Figs. 5 and 6 will be incipient stages of atomic ordering that eventually forms the tetragonal lattice (1). The structure shown in Figs. 7 and 8 is an intermediate stage between the structures represented by Figs. 5 and 4. The process of atomic ordering at the interfaces between the Bi and Mn layers can thus be divided into two stages. In the first stage, Mn atoms combine with Bi atoms, which are in threefold symmetry on its (001) surface, to form clusters of twelvefold symmetry that appear as the doughnut-shaped contrasts in Fig. 5. This stage corresponds to building up of short-range atomic order. Formation of such polyatomic clusters in quasicrystal formation has been proposed by Audier & Guyot (1988) in considering a prior stage to the development of long-range cluster linkages in the icosahedral Al_6CuLi_3 phase. The doughnut-shaped white contrasts in Fig. 5 have a diameter of about 16 Å and may constitute a real example of such polyatomic clusters.

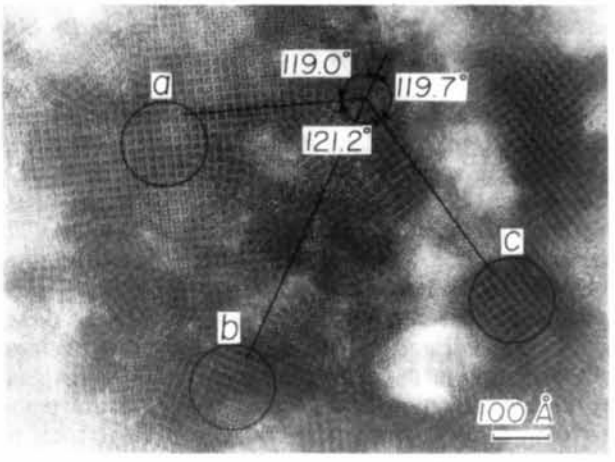

Fig. 7. High-resolution structure image of a specimen prepared in a vacuum of 10^{-8} Torr ($1{\cdot}33 \times 10^{-6}$ Pa) and heated at 513 K for 100 h in the same vacuum.

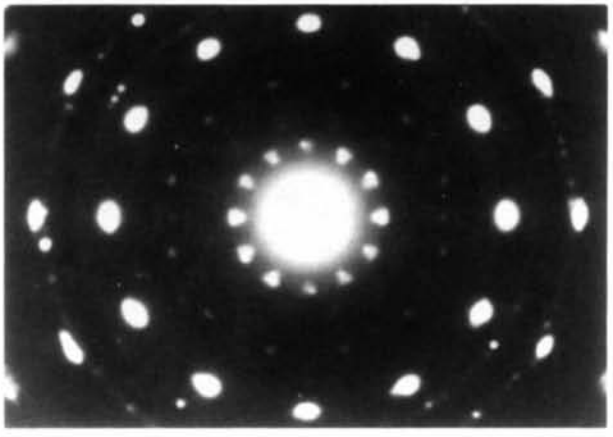

Fig. 8. Electron diffraction pattern confirming the structural features seen in Fig. 7. This pattern was taken from another area of the same specimen as that in Fig. 4.

In the second stage, these clusters arrange themselves to form the tetragonal long-range order, as seen in the small regions, *a*, *b* and *c*, in Fig. 7. The fact that such tetragonal regions always take trigonal orientations supports the above conclusion that the polyatomic Bi–Mn clusters in the first stage have twelvefold symmetry. In comparing the square unit patterns in Fig. 4 (more clearly in Fig. 7) with the doughnut-shaped contrasts in Fig. 5, it seems that a little deformation will be necessary for the clusters to build up the tetragonal lattice in the second stage, in order to satisfy the lowering of symmetry from twelve- to fourfold, as was also suggested by Audier & Guyot (1988).

References

AUDIER, M. & GUYOT, P. (1988). *Proc. 5th Jpn Inst. Met. Int. Symp. (JIMIS-5) Non-Equilibrium Solid Phases Met. Alloys*, Kyoto, 1988, p. 467.

CHEN, D. (1971). *J. Appl. Phys.* **42**, 3625–3628.

HONDA, S. & KUSUDA, T. (1974). *J. Appl. Phys.* **45**, 2689–2692.

IWAMA, Y., MIZUTANI, U. & HUMPHREY, F. B. (1972). *IEEE Trans. Magn.* **8**, 487–489.

UNGER, Y. & STOLZ, M. (1971). *J. Appl. Phys.* **42**, 1085–1089.

WILLIAMS, H. J., SHERWOOD, R. C., FOSTER, F. G. & KELLEY, E. M. (1957). *J. Appl. Phys.* **28**, 1181–1184.

YOSHIDA, K., YAMADA, T. & FURUKAWA, Y. (1986). *Acta Metall.* **34**, 969–979.

YOSHIDA, K., YAMADA, T. & TANIGUCHI, Y. (1987). *14th Int. Congr. Crystallogr.*, Perth, 1987. Collected Abstracts, p. C-123.

Acta Cryst. (1989). B**45**, 45–52

Electron Density, Thermal Motion and Bonding Interactions in the Perovskite Structures KMF_3 with M = Mn, Fe, Co and Ni

BY E. N. MASLEN AND N. SPADACCINI

Crystallography Centre, University of Western Australia, Nedlands 6009, *Australia*

(*Received* 17 *July* 1988; *accepted* 20 *September* 1988)

Abstract

The KMF_3 structures with M = Mn, Fe, Co and Ni have been investigated in detail using data from previous studies. The vibration amplitudes, atomic charges determined by difference density partitioning and the heights of characteristic features of the difference densities change monotonically through the series. Trends in the difference densities are consistent with the expected variation of the exchange contribution (antisymmetrization of the electron wavefunction) with the occupancy of the 3*d* subshell. The redistribution of electron density in the region of overlap of the atomic orbitals for the transition-metal and F atoms reflects mainly the effects of that exchange. The topography also shows the consequences of interactions between the transition-metal and the next-nearest-neighbour K atoms. There are local maxima or minima in the difference densities further from the nuclei. The sign of the difference density at these regions of low electrostatic potential depends on the chemical identity of the M species.

Introduction

Information contained in difference electron densities from X-ray diffraction experiments extends our understanding of chemical bonding. The detailed three-dimensional image of the electron density from an accurate diffraction experiment provides a benchmark against which the validity of models for chemical bonding can be tested. At a qualitative level the predictions of the model can be checked for consistency with the topography of the electron density. The ultimate objective is to predict properties as completely as possible from the one electron density function.

The simplest case is that of a series of isomorphous compounds in which only one type of atom varies. The environment remains approximately constant if the electronic structure of just one atom changes. The Mn, Fe, Co and Ni members of the KMF_3 series crystallize in the cubic space group $Pm3m$ and with the ideal perovskite structure (Wyckoff, 1964). The atoms are located at the special positions M(0,0,0), K($\frac{1}{2},\frac{1}{2},\frac{1}{2}$) and F($\frac{1}{2}$,0,0) and have low temperature factors. The transition metal is coordinated to six F atoms in an ideal octahedron. The second-nearest neighbours consist of eight K atoms located in the $\langle 111 \rangle$ directions of that octahedron. Difference densities for these compounds have been described earlier (Kijima, Tanaka & Marumo, 1981, 1983; Miyata, Tanaka & Marumo, 1983). Those studies accurately displayed the rearrangement of the transition-metal *d* electrons as a result of the crystal field and determined relative populations for the t_{2g} and e_g orbitals. The magnitude of the redistribution of electron density increases progressively through the series, in line with the increase in the polarizability expected for the transition metal.

0108-7681/89/010045-08$03.00